We are IntechOpen, the world's leading publisher of Open Access books Built by scientists, for scientists

6,900
Open access books available

185,000
International authors and editors

200M
Downloads

Our authors are among the

154
Countries delivered to

TOP 1%
most cited scientists

12.2%
Contributors from top 500 universities



WEB OF SCIENCE™

Selection of our books indexed in the Book Citation Index in Web of Science™ Core Collection (BKCI)

Interested in publishing with us?
Contact book.department@intechopen.com

Numbers displayed above are based on latest data collected.
For more information visit www.intechopen.com



Chapter 4

Stator-Flux-Oriented Sliding Mode Control for Doubly Fed Induction Generator

Ivan Villanueva, Antonio Rosales, Pedro Ponce and Arturo Molina

Additional information is available at the end of the chapter

http://dx.doi.org/10.5772/intechopen.70714

Abstract

Doubly-fed induction generator (DFIG) is the most implemented electric machine in wind energy conversion systems (WECSs) due to reduced size converter, active and reactive power control, and economic factors. However, the power electronic stage needs an accurate controller that allows to follow the stator power regulation despite the presence of disturbances. On the other hand, sliding-mode control (SMC) offers a fast-dynamic response and provides insensitivity to matched and bounded disturbance/uncertainties, and its natural discontinuous control signals can be used for direct switching of power electronic devices. Switching frequency must be maintained inside acceptable values to avoid exceeding the maximum admissible switching frequency of semiconductors. The contribution of this chapter is a stator-flux–oriented SMC with a hysteresis band that limits the switching frequency of power electronic devices to a set value. Furthermore, the proposed SMCs ensure robustness against bounded low-voltage grid faults. Unlike other nonmodulated techniques like direct torque control (DTC), there is no necessity of modifying the controller structure for withstanding low-depth voltage dips. The controller injects negative sequence voltage/currents to compensate the unbalanced conditions. The advantages of the proposed SMC control are validated via simulations.

Keywords: doubly-fed induction generator, sliding mode control

1. Introduction

In recent years, wind energy has been established as the fastest growing energy source among renewables. From a global perspective, more than 90 countries have been involved in the installation of new renewable wind power plants [1]. In 2015, the new global installed capacity hit the record for an increase of approximately 64 GW. During 2016, more than 54 GW were

INTECH
open science | open minds

© 2018 The Author(s). Licensee InTech. This chapter is distributed under the terms of the Creative Commons Attribution License (http://creativecommons.org/licenses/by/3.0), which permits unrestricted use, distribution, and reproduction in any medium, provided the original work is properly cited. CC BY

installed for a total of approximately 487 GW by the end of 2016. Conservative prognoses forecast an increment of 60 GW in 2017 with a continuous annual grow of about 75 GW by 2021. With the continued improvement in wind turbines technology and ecological concerns, the wind power is now a serious competitor against heavily subsidized energy industries [1, 2].

Doubly-fed induction generator (DFIG) is a wound-rotor induction machine with voltage injection in the rotor winding. This allows a limited speed control of the electric machine, which is sufficient to implement maximum aerodynamic efficiency by maintaining the tip-speed ratio at the nominal value at most operational conditions of the turbine.

The success of DFIG in wind energy applications lies in the reduced power converter, which is typically about 25–30% of the nominal power of the electric machine; furthermore, by current injection in the rotor, it is possible to control the reactive power injected to the electric grid, which is very important for minimizing cooper loses or reactive power compensation [3]. More than 70% of the installed wind turbines use DFIG. However, this machine is very sensitive to voltage variations in the grid because the stator is directly connected to the grid [4], in contrast to other variable-speed machines that are connected through a full-size power converter.

Sliding mode control (SMC) is a nonlinear control technique that ensures finite-time convergence of the sliding surface to zero guarantying robustness against bounded disturbances and parameter variations [9]. The main disadvantage of SMC is the chattering effect (high frequency oscillations with finite amplitude) caused by unmodeled dynamics and discretization [9]. On the other hand, power electronics are controlled by means of the injection of discontinuous signals matching with the discontinuous nature of conventional SMC; therefore, conventional SMC can be used for direct switching of power electronics on DFIG applications, avoiding modulation. SMC has been successfully implemented in DFIG control and tested under unbalanced conditions and harmonics [11, 15–18]. However, the proposals given in [16, 17] require modulation, and the tested faults are moderate since these do not represent a brusque variation in the stator voltage. The SMC presented in [15–18] works under unbalanced conditions but implementation of the SMC regarding the commutation of the power electronics is not discussed.

In this chapter, it is presented a SMC with the following advantages: (a) do not required modulation; (b) do not require modifications of the controller structure to withstand stator voltage perturbances (compared with classical control approach as direct-torque-control [DTC], see [5]); and (c) the controller can regulate torque and reactive power even under unbalanced conditions, which is equivalent to negative current regulation. Therefore, the proposed SMC offers a very simple alternative that requires neither symmetrical decomposition nor pulse width modulation and is not affected by parameter variation. Furthermore, the DFIG system with SMC is characterized in the frequency domain for estimating the commutation frequency of power electronics. A maximum switching frequency value is ensured by means of the addition of hysteresis in the sign function. The hysteresis value is computed applying the Tsypkin's method, a theoretically exact technique to analyze nonlinear systems [12, 14]. Due to the nature of the power converter, the voltage gain seen by the controller is variable in time, which makes difficult to maintain the switching frequency constant. However, it is possible to compute a maximum switching frequency value (minimum hysteresis value), which provides a commutation frequency inside of the acceptable values given in the datasheet of the power electronics.

http://dx.doi.org/10.5772/intechopen.70714

The chapter presents the dynamic modeling of the electric machine and the wind turbine, the controller design, frequency domain characterization, and finally, fault-ride through capability is evaluated analyzing the regulated current from a sequence components point of view.

2. Aerodynamic model of wind turbine

Horizontal axis wind turbines are used to extract mechanical power from the wind resource based on the lifting force of the rotor blades. The mechanical power is a function of the kinematic energy of the wind and the power coefficient:

$$P_{wind} = \frac{1}{2} C_P(\Lambda, \gamma) \rho A V^3 \tag{1}$$

The power coefficient is a function of the tip speed ratio and the pitch angle. Since very complex aerodynamic analyses are required to characterize turbine blades, the power coefficient is usually approximated using mathematical expressions such as [7]:

$$C_P = c_1(c_2\kappa - c_3\gamma - c_4\gamma^{c_5} - c_6)e^{-c7\kappa} \tag{2}$$

where $\kappa = \frac{1}{\Lambda + 0.06\ \gamma} - \frac{0.035}{1+\gamma^3}$ and c_1 to c_7 are coefficients dependent on the blades geometry.

The tip speed ratio is the relationship between the tangential speed of the blades tip and the wind speed if it is expressed using the DFIG mechanical speed and the gearbox ratio we obtain:

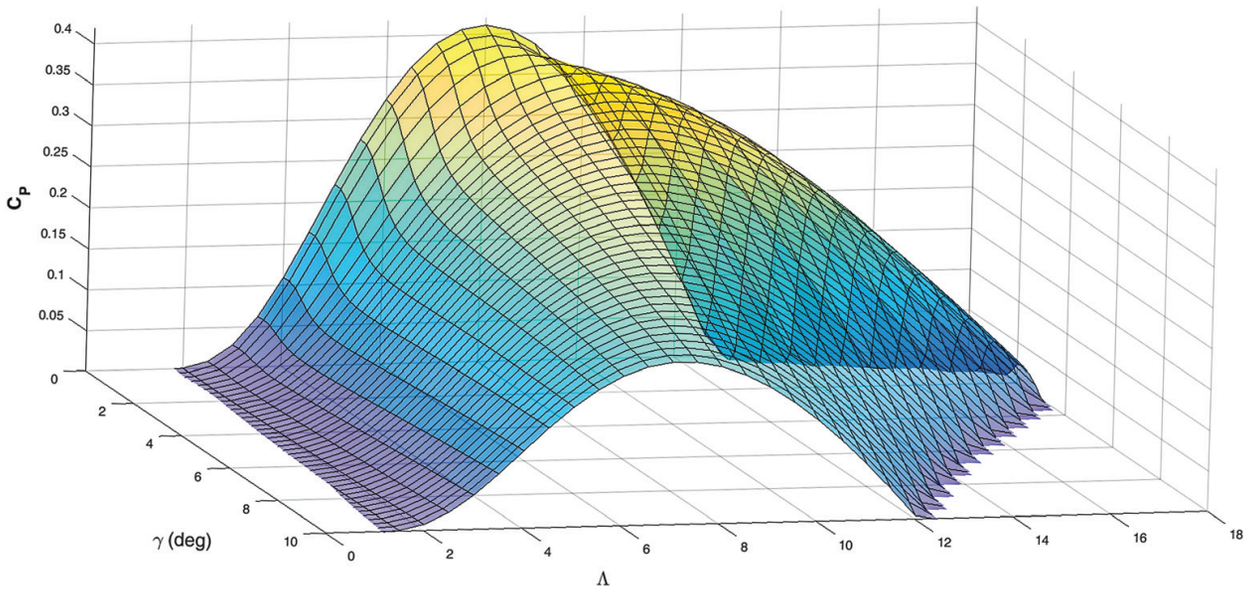


Figure 1. Power coefficient as a function of tip speed ratio and pitch angle.

$$\Lambda = \frac{\omega_m r}{\eta V} \tag{3}$$

Pitch angle is normally used for aerodynamically reduce power extraction when the wind speed is above the nominal value. For normal operation, it is maintained constant, while the rotor speed is controlled by the DFIG to maintain the tip speed ratio constant, for the blades model shown in **Figure 1**, the nominal pitch angle is zero and the nominal tip speed ratio is 8 for a maximum power coefficient of approximately 0.41. The parameters used to generate the displayed function are $c_1 = 0.5$; $c_2 = 116$; $c_3 = 0.4$; $c_4 = 0$; $c_6 = 5$; $c_7 = 21$:

3. Dynamic modeling of the DFIG

The dynamic equivalent circuit of DFIG can be expressed in an arbitrary reference frame rotating at a speed equal to ω [6, 8]:

$$v_{sd} = \frac{d\lambda_{sd}}{dt} - \omega\lambda_{sq} + R_s i_{sd} \tag{4}$$

$$v_{sq} = \frac{d\lambda_{sq}}{dt} + \omega\lambda_{sd} + R_s i_{sq} \tag{5}$$

$$v_{rd} = \frac{d\lambda_{rd}}{dt} - (\omega - \omega_m)\lambda_{rq} + R_r i_{rd} \tag{6}$$

$$v_{rq} = \frac{d\lambda_{rq}}{dt} + (\omega - \omega_m)\lambda_{rd} + R_r i_{rq} \tag{7}$$

$$\lambda_{sd} = L_s i_{sd} + L_m i_{rd} \tag{8}$$

$$\lambda_{sq} = L_s i_{sq} + L_m i_{rq} \tag{9}$$

$$\lambda_{rd} = L_r i_{rd} + L_m i_{sd} \tag{10}$$

$$\lambda_{rq} = L_r i_{rq} + L_m i_{sq} \tag{11}$$

The electromagnetic torque can be expressed as an interaction between rotor current and stator magnetic flux:

$$T_{em} = \frac{3PL_m}{2L_s}\left(i_{rd}\lambda_{sq} - i_{rq}\lambda_{sd}\right) \tag{12}$$

A common expression of the stator reactive power in terms of the stator voltage and rotor current is:

$$Q_s = \frac{3L_m}{2L_s}\left(v_{sd}i_{rq} - v_{sq}i_{rd}\right) + \frac{3}{2L_s}\left(\lambda_{sd}v_{sq} - \lambda_{sq}v_{sd}\right) \tag{13}$$

The second term of Eq. (13) is the reactive power required to magnetize the electric machine.

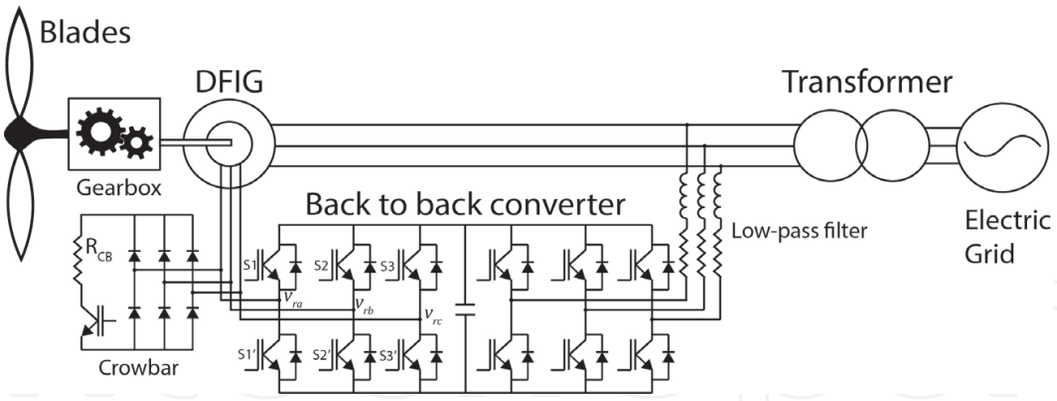


Figure 2. Basic scheme of DFIG-based wind turbine.

The basic scheme of a wind turbine is shown in **Figure 2**. A back-to-back power converter is necessary to send the required voltage to the rotor. In the grid side, it is also necessary a converter since the power flow must be bidirectional, from the electric machine to the grid at super-synchronous operation of the machine and from the electric grid to the machine at sub-synchronous operation. Grid side converter is usually controlled by cascade controller, which maintains DC-link voltage constant by regulating the grid current. The reactive power can also be controlled; hence, the wind turbine operates at unitary power factor, or it can inject reactive power to the grid similarly to an electrically excited synchronous generator. For purposes of this work, let us consider that the DC-link voltage is maintained constant by the grid-side controller.

3.1. Rotor-side power converter model

DFIG rotors are typically connected in star with the neutral connection isolated, the voltage if measured from phase a to the neutral point of the rotor star will be a combination of the phase voltages, which can be summarized using the following matrix equation:

$$\begin{bmatrix} v_{an} \\ v_{bn} \\ v_{cn} \end{bmatrix} = \frac{V_{DC}}{3} \begin{bmatrix} 2 & -1 & -1 \\ -1 & 2 & -1 \\ -1 & -1 & 2 \end{bmatrix} \overbrace{\begin{bmatrix} S_1 \\ S_2 \\ S_3 \end{bmatrix}}^{S_{123}} \tag{14}$$

Each component of the vector $S_{1,2,3}$ has only two valid states, 0 or 1. Then, each phase voltage has six different possible values: $\pm\frac{2}{3}V_{DC}$, $\pm\frac{1}{3}V_{DC}$, 0. The rotor side converter can be analyzed as a discontinuous sign function with variable gain.

4. Sliding mode controller design

It is well known from vector control that orienting the machine model presented in Section 3 in the stator flux reference frame is an effective way for decoupling active power (or torque) and reactive power control by means of rotor current regulation. In normal operation, the stator

voltage vector will lead the stator flux by approximately 90 degrees neglecting voltage drop due to the stator resistance. From Eqs. (12) and (13) oriented at the stator flux direction, i.e., $\lambda_{sq}=0$ and $v_{sd}=0$, we obtain a decoupled control system: $T_{em} = -\frac{3PL_m}{2L_s}\lambda_{sd}\boldsymbol{i_{rq}}$ and $Q_s = -\frac{3L_m}{2L_s}v_{sq}\boldsymbol{i_{rd}} + \frac{3}{2L_s}\lambda_{sd}v_{sq}$. However, under unbalanced conditions, the phase shift between voltage and flux will not be constant; therefore, robust control is necessary to withstand this perturbation.

From Eq. (8), the direct axis component of stator current can be expressed as:

$$i_{sd} = \frac{\lambda_{sd} - L_m i_{rd}}{L_s} \tag{15}$$

Substituting Eq. (15) in Eq. (10):

$$\lambda_{rd} = L'_r i_{rd} + \frac{L_m}{L_s}\lambda_{sd} \tag{16}$$

where $L'_r = L_r - \frac{L_m^2}{L_s}$.

The quadrature component of rotor flux can be obtained in a similar way:

$$\lambda_{rq} = L'_r i_{rq} + \frac{L_m}{L_s}\lambda_{sq} \tag{17}$$

Substituting Eqs. (16) and (17) in (6) and (7) and solving for $\frac{di_{rd}}{dt}$ and $\frac{di_{rq}}{dt}$:

$$\frac{di_{rd}}{dt} = \frac{1}{L'_r}\left(v_{rd} - R_r i_{rd} - \frac{L_m}{L_s}\frac{d\lambda_{sd}}{dt} + \omega_r L'_r i_{rq} + \frac{L_m}{L_s}\omega_r\lambda_{sq}\right) \tag{18}$$

$$\frac{di_{rq}}{dt} = \frac{1}{L'_r}\left(v_{rq} - R_r i_{rq} - \frac{L_m}{L_s}\frac{d\lambda_{sq}}{dt} - \omega_r L'_r i_{rd} - \frac{L_m}{L_s}\omega_r\lambda_{sd}\right) \tag{19}$$

where $\omega_r = \omega_s - \omega_m$. Since the reference frame selected rotate at a synchronous speed, ω_r is equivalent to the rotor current angular speed and the slip angular frequency.

In **Figure 3**, the equivalent system for current regulation is shown. Under normal operation, the stator flux induces a voltage in the quadrature axis loop. The induced voltage is proportional to the slip and affects only the active power (or torque) regulation loop. Under a grid fault, the stator flux is directly affected and can be analyzed as another perturbation affecting the current regulation. Analyzing the flux in positive, negative, and natural fluxes, we can see the influence of the induced voltage (perturbation) to the current regulation loop. The positive sequence flux has an induced voltage proportional to $s\omega_s$, the slip is less than 0.3 for this type of machine; therefore, the induced voltage is low. The natural flux does not rotate; therefore, the induced voltage is proportional to the mechanical speed of the machine, and the negative flux rotates opposite to the reference frame orientation, the induced voltage is very large, proportional to near twice the synchronous speed $(2-s)\omega_s$ [8]. If the grid fault is very large, no control strategy could withstand this kind of perturbation, since the induced voltage may be larger than the rotor voltage. For that reason, external protection devices are required, and the simplest one is the crowbar.

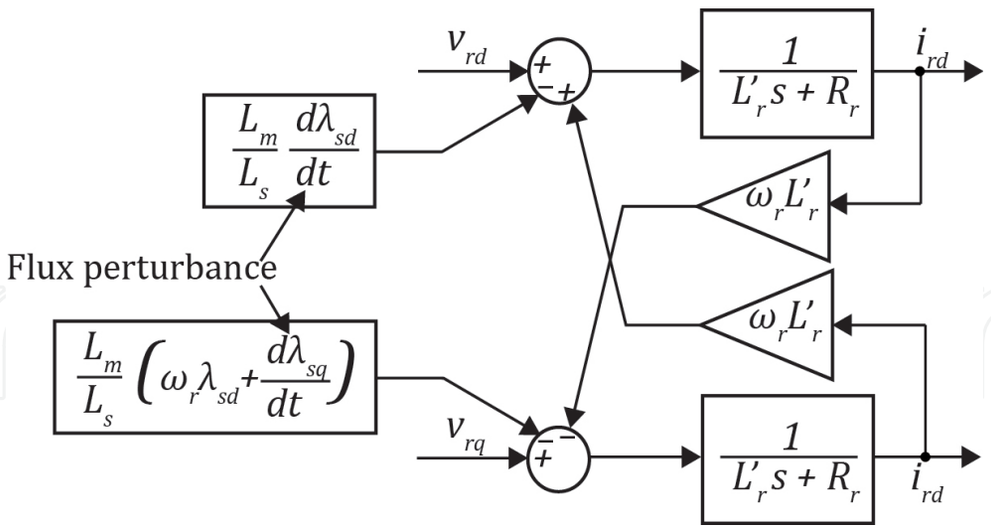


Figure 3. Equivalent current plant including stator flux perturbation.

SMC is robust against bounded disturbances and parameter variations; hence, it is a good alternative to control perturbed plants as the DFIG model shown in **Figure 3**. As we want to control the torque and reactive power, the following sliding surfaces are selected:

$$\sigma_{T_{em}} = T_{em} - T^*_{em}; \qquad \sigma_{Q_s} = Q_s - Q^*_s \tag{20}$$

where T^*_{em} and Q^*_s are the desired (reference) value of torque and reactive power, considering that the reference values are much slower than the dynamics of the system and that the stator flux is perfectly aligned with the reference frame d axis:

$$\dot{\sigma}_{T_{em}} = \dot{T}_{em} = -\frac{3PL_m}{2L_s}\left(\dot{i}_{rq}\lambda_{sd} + i_{rq}\dot{\lambda}_{sd}\right) \tag{21}$$

On the other hand, the voltage vector may have a d component due to voltage perturbation:

$$\dot{\sigma}_{Q_s} = \dot{Q}_s = \frac{3L_m}{2L_s}\left(\dot{v}_{sd}i_{rq} + v_{sd}\dot{i}_{rq} - \dot{v_{sq}}i_{rd} - v_{sq}\dot{i}_{rd}\right) + \frac{3}{2L_s}\left(\dot{\lambda}_{sd}v_{sq} + \lambda_{sd}\dot{v}_{sq}\right) \tag{22}$$

Substituting Eqs. (18) and (19) in (22) and (23):

$$\dot{\sigma}_{T_{em}} = \overbrace{kP\lambda_{sd}\left(R_r i_{rq} + \frac{L_m}{L_s}\omega_r\lambda_{sd} + \omega_r L'_r i_{rd}\right)}^{F_{T_{em}}} \overbrace{-kP\lambda_{sd}v_{rq}}^{d_{T_{em}}} \overbrace{-kPL'_r i_{rq}\dot{\lambda}_{sd}}^{P_{T_{em}}} \tag{23}$$

$$\dot{\sigma}_{Q_s} = \overbrace{kv_{sq}\left(R_r i_{rq} - \omega_r L'_r i_{rq}\right)}^{F_{Q_s}} \overbrace{-kv_{sq}v_{rd}}^{d_{Q_s}} + \underbrace{kv_{sq}\left[\frac{L_m}{L_s}\dot{\lambda}_{sd} + \frac{L'_r}{v_{sq}}\left(\dot{v}_{sd}i_{rq} + v_{sd}\dot{i}_{rq} - \dot{v_{sq}}i_{rd}\right)\right] + \frac{3}{2L_s}\left(\dot{\lambda}_{sd}v_{sq} + \lambda_{sd}\dot{v}_{sq}\right)}_{P_{Q_s}} \tag{24}$$

where $k = \frac{3L_m}{2L_sL_r}$, expressing Eqs. (23) and (24) in matrix form:

$$\begin{bmatrix} \dot{\sigma}_{T_{em}} \\ \dot{\sigma}_{Q_s} \end{bmatrix} = \begin{bmatrix} F_{T_{em}} \\ F_{Q_s} \end{bmatrix} - k \begin{bmatrix} 0 & P\lambda_{sd} \\ v_{sq} & 0 \end{bmatrix} \begin{bmatrix} v_{rd} \\ v_{rq} \end{bmatrix} + \begin{bmatrix} P_{T_{em}} \\ P_{Q_s} \end{bmatrix} \tag{25}$$

Under normal conditions, all the terms dependent on $v_{sd}, \dot{v}_{sd}, \dot{v}_{sq}$ and $\dot{\lambda}_{sd}$ are equal to zero. Under abnormal conditions those terms can be analyzed as perturbations $P_{T_{em}}$ and P_{Q_s}. The control signals v_{rd} and v_{rq} appears in the first derivate of the sliding surface, thus the relative degree of the control system is one. Then, finite time convergence to the sliding surface and robustness against bounded disturbance/uncertainties can be achieved using the control signal:

$$\begin{bmatrix} v_{rd} \\ v_{rq} \end{bmatrix} = \begin{bmatrix} -M_d \operatorname{sgn}\left(\sigma_{Q_s}\right) \\ -M_q \operatorname{sgn}\left(\sigma_{T_{em}}\right) \end{bmatrix} \tag{26}$$

where $M_d, M_q > 0$. A detailed description of M_d and M_q computation is given in section 4.1.

Remark: A discontinuous function is intentionally selected because the nature of the rotor-side power converter is discontinuous as well; therefore, the control signal can be easily used directly from the controller algorithm to the power converter without modulation. On the contrary, any continuous control; e.g. saturation, sigmoid function, etc. employed to smooth the discontinuous control in Eq. (26) must be modulated to be implementable in a power converter; therefore, chattering will be present no matter the control strategy used.

The desired voltage need to be send through the rotor-side power converter. The voltage seen from the stator flux reference frame is obtained using park transform:

$$\begin{bmatrix} v_{rd} \\ v_{rq} \end{bmatrix} = \overbrace{\begin{bmatrix} \cos\theta_d & -\sin\theta_d \\ \sin\theta_d & \cos\theta_d \end{bmatrix} \frac{2}{3} \begin{bmatrix} 1 & -1/2 & -1/2 \\ 0 & \sqrt{3}/2 & -\sqrt{3}/2 \end{bmatrix}}^{T} \begin{bmatrix} v_{an} \\ v_{bn} \\ v_{cn} \end{bmatrix} \tag{27}$$

where the reference frame angle is $\theta_d = \theta_m - \theta_{sf}$.

Using Eqs. (14) (25) and (27), it is possible to establish a relationship between *dq* and *abc* quantities:

$$\begin{bmatrix} \sigma_{T_{em}} \\ \sigma_{Q_s} \end{bmatrix} = \overbrace{-k \begin{bmatrix} 0 & P\lambda_{sd} \\ v_{sq} & 0 \end{bmatrix} T \frac{V_{DC}}{3} \begin{bmatrix} 2 & -1 & -1 \\ -1 & 2 & -1 \\ -1 & -1 & 2 \end{bmatrix}}^{D} \begin{bmatrix} \sigma_a \\ \sigma_b \\ \sigma_c \end{bmatrix} \tag{28}$$

Since the matrix D is not square, the Moore-Penrose pseudo-inverse is used:

$$\overbrace{\begin{bmatrix} \sigma_a \\ \sigma_b \\ \sigma_c \end{bmatrix}}^{\sigma_{abc}} = D^{+} \begin{bmatrix} \sigma_{T_{em}} \\ \sigma_{Q_s} \end{bmatrix} \tag{29}$$

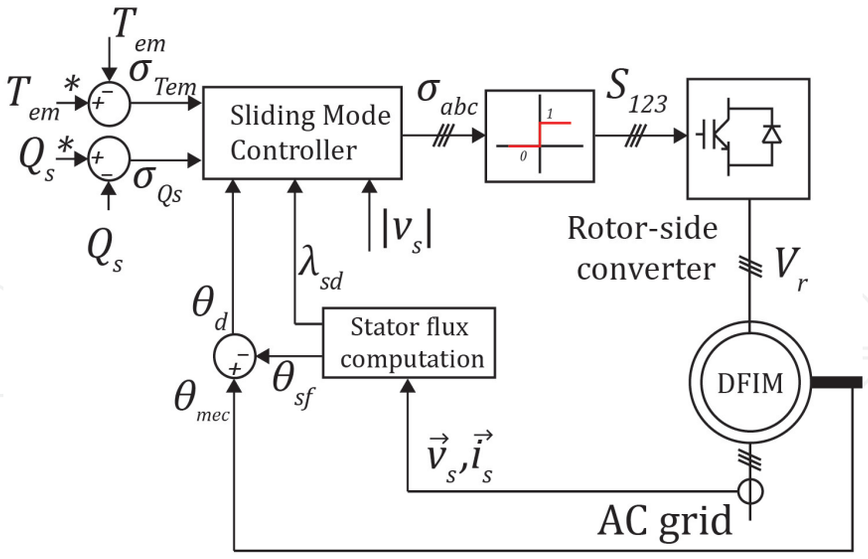


Figure 4. Basic scheme of SMC.

where:

$$D^{+} = D^{T}\left(DD^{T}\right)^{-1} = -\frac{3}{kV_{DC}}\begin{bmatrix} \frac{1}{P\lambda_{sd}}\sin\theta_d & \frac{1}{v_{sq}}\cos\theta_d \\ \frac{1}{P\lambda_{sd}}\sin\left(\theta_d + 2\pi/3\right) & \frac{1}{v_{sq}}\cos\left(\theta_d + 2\pi/3\right) \\ \frac{1}{P\lambda_{sd}}\sin\left(\theta_d - 2\pi/3\right) & \frac{1}{v_{sq}}\cos\left(\theta_d - 2\pi/3\right) \end{bmatrix}$$

The constant term $\frac{3}{kV_{DC}}$, which contains parameters of the electric machine, can be removed from the transformation matrix, since the controller will only evaluate the sign of σ_{abc}, thus the controller is robust against parametric uncertainties; under normal conditions, the stator flux direct component (λ_{sd}) and stator voltage quadrature component (v_{sq}) are constant. In **Figure 4** is shown the basic scheme of the presented controller. The output of Eq. (29) is the equivalent *abc* sliding surface, then a function similar to sign is used to evaluate the switch state (0 means lower leg activated and 1 means upper leg activated). The resulting control system does not require modulation since the switching state is determined directly from the control system.

4.1. Sliding mode existence condition

For a relative degree one system

$$\dot{\sigma} = F(x) + d(x)u \qquad (x \in \mathbb{R}^n) \tag{30}$$

With a scalar control

$$u = -M\,\mathrm{sgn}\,(\sigma) \tag{31}$$

The condition for satisfying the existence of the sliding mode is [9]:

$$d(x)M > |F(x)| \tag{32}$$

The stator-flux–oriented SMC has a very similar form of system of Eq. (30). Then, existence of SMC is ensured if the following conditions are met:

$$M_{q,min} > |(F_{T_{em}} + P_{T_{em}})/d_{T_{em}}|; \circledcirc M_{d,min} > |(F_{Q_s} + P_{Q_s})/d_{Q_s}| \tag{33}$$

Therefore, choosing M_d and M_q using Eq. (33) ensures finite convergence to the sliding variable and insensitivity to bounded disturbance/uncertainties. The only requirement to compute the gains M_d and M_q is the knowledge of the bounds of the system and the disturbance/uncertainties, $|F_{Q_s,T_{em}}|$, $|d_{Q_s,T_{em}}|$ and $|P_{Q_s,T_{em}}|$. Note that real implementation of control gains in Eqs. (33) depends of DC-link voltage V_{DC}, which is variable in practice, and it must be ensured that V_{DC} is regulated correctly to ensure a robust performance of the rotor side of the DFIG system.

4.2. Switching frequency limitation

In **Figure 4** it is shown the scheme of an ideal sliding mode controller; however, it requires infinite switching frequency, which is not possible in real physical systems, therefore, the most common solution for this issue is to include a hysteresis loop to the ideal sign function [10] since hysteresis makes the switching frequency finite. Note that sigmoid functions and saturation can be implemented to reduce switching frequency as well as attenuate chattering. However, these functions are continuous and/or contain linear parts requiring modulation for its application to power electronics, while a sign function with hysteresis can be injected without modulation.

A widely used method to determine limit cycles and the oscillation frequency is the sinusoidal describing function (DF), which can be used for segmented nonlinear system composed by a linear system and a nonlinear part [12], that is the case of a linear plant controlled by a relay-based control system (see **Figure 5**). A requirement for applying DF is that the linear system $L(s)$ must have a low-pass filter behavior. Furthermore, only the first harmonic is considered in the analysis. However, for relative degree-one systems as the one presented in this chapter, this technique is not suitable [12]. DF will predict no oscillations because it ignores the contribution of the harmonics. On the other hand, Tsypkin's method is an exact method in which one can

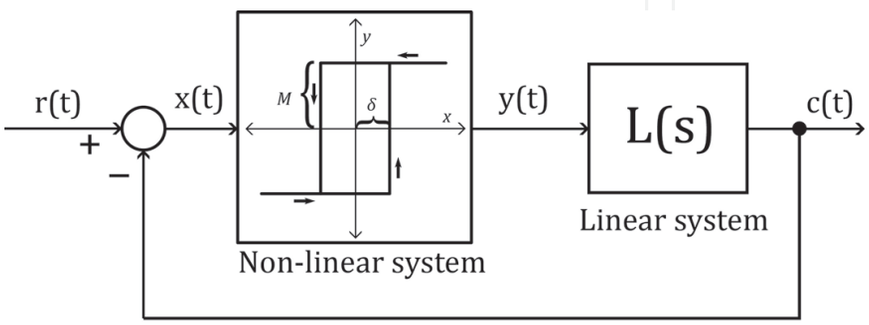


Figure 5. Relay-based control of a linear system.

select the number of harmonics to be considered, and it can be applied to estimate oscillations in relative degree one systems. Therefore, the DFIG system with SMC presented in this chapter is analyzed in the frequency domain using Tsypkin's method.

Expressing Eqs. (4)–(11) in matrix form:

$$\dot{x} = Ax + Bu; \qquad y = Cx \tag{34}$$

where:

$x = \begin{bmatrix} i_{sd} & i_{sq} & i_{rd} & i_{rq} \end{bmatrix}^T$; $u = \begin{bmatrix} v_{sd} & v_{sq} & v_{rd} & v_{rq} \end{bmatrix}^T$;

$$A = \frac{1}{L_r' L_s} \begin{bmatrix} -R_s L_r & \omega_m L_m^2 + \omega_s L_r' L_s & R_r L_m & \omega_m L_m L_r \\ -\omega_m L_m^2 - \omega_s L_r' L_s & -R_s L_r & -\omega_m L_m L_r & R_r L_m \\ R_s L_m & -\omega_m L_s L_m & -R_r L_s & -\omega_m L_r L_s + \omega_s L_r' L_s \\ \omega_m L_s L_m & R_S L_m & \omega_m L_r L_s - \omega_s L_r' L_s & -R_r L_s \end{bmatrix};$$

$$B = \frac{1}{L_r' L_s} \begin{bmatrix} L_r & 0 & -L_m & 0 \\ 0 & L_r & 0 & -L_r \\ -L_m & 0 & L_s & 0 \\ 0 & -L_m & 0 & L_s \end{bmatrix}; C = \begin{bmatrix} 0 & 0 & 1 & 0 \\ 0 & 0 & 0 & 1 \end{bmatrix}.$$

The system presents a nonlinearity due to the mechanical speed ω_m, which is dependent on the electromagnetic torque and the mechanical equation; however, since the time scales of the electrical quantities is much smaller than the time scale of the mechanical system, we are going to study system of Eq. (34) as a set of linear systems varying the mechanical speed in a range of ±30% about the synchronous speed. Other supposition is that the system is fully decoupled, that is, v_{rd} controls i_{rd} and v_{rq} controls i_{rq}. So, we can obtain both transfer functions from the diagonal elements of the following matrix equation:

$$G(\mathcal{s}) = C(\mathcal{s}I - A)^{-1}B + D \tag{35}$$

where I is a 4 x 4 identity matrix. The diagonal transfer functions will be relative degree one systems with four poles and three zeros:

$$L(\mathcal{s}) = \frac{I_{rd}(\mathcal{s})}{V_{rd}(\mathcal{s})} = \frac{I_{rq}(\mathcal{s})}{V_{rq}(\mathcal{s})} = \frac{a_3\mathcal{s}^3 + a_2\mathcal{s}^2 + a_1\mathcal{s} + a_0}{d_4\mathcal{s}^4 + d_3\mathcal{s}^3 + d_2\mathcal{s}^2 + d_1\mathcal{s} + d_0} \tag{36}$$

Tsypkin's locus is defined as [12]:

$$T(j\omega) = \sum_{n\ odd}^{\infty} \mathrm{Re}[L_1(jn\omega)] + j \sum_{n\ odd}^{\infty} \frac{1}{n} \mathrm{Im}[L_1(jn\omega)] \tag{37}$$

The conditions required to predict a limit cycle oscillating at an angular frequency ω_0 are [12]:

$$\mathrm{Im}[T(j\omega_0)] = \frac{\pi}{4}\left[L(\infty) - \frac{\delta}{M}\right] \tag{38}$$

$$\mathrm{Re}[T(j\omega_0)] < \frac{\pi}{4\omega_0}\lim_{s\to\infty}[sL_1(s)] \tag{39}$$

In **Figure 6** it is shown the graphical solution for a DFIG with the characteristics shown in **Table 1**, the mechanical speed has minor influence at high frequencies; therefore, it is valid to consider the DFIG as a linear system (note that the number of pole pairs is not considered in (34); therefore, the mechanical speed reported is the one of an equivalent two pole machine). Supposing that the power inverter has a maximum switching frequency of $f_{max} = 4000$ Hz $\rightarrow$ $\omega_0 = 8000\pi\,\frac{\mathrm{rad}}{\mathrm{s}}$, from Eq. (38), we can calculate the hysteresis width. We know that the maximum gain the system can have is $M_{max} = \frac{2}{3}V_{dc}$, then the hysteresis loop that will ensure a maximum switching frequency of 4000 Hz is:

$$\delta = \frac{(0.3094)(4)}{\pi} * \frac{2}{3}600 = 157.57\ A$$

However, the control system was designed to direct control torque and reactive power, so we need to calculate the hysteresis width of those quantities, which can be easily done since the control system is decoupled, and the current direct and quadrature components are directly related with reactive power and torque, respectively.

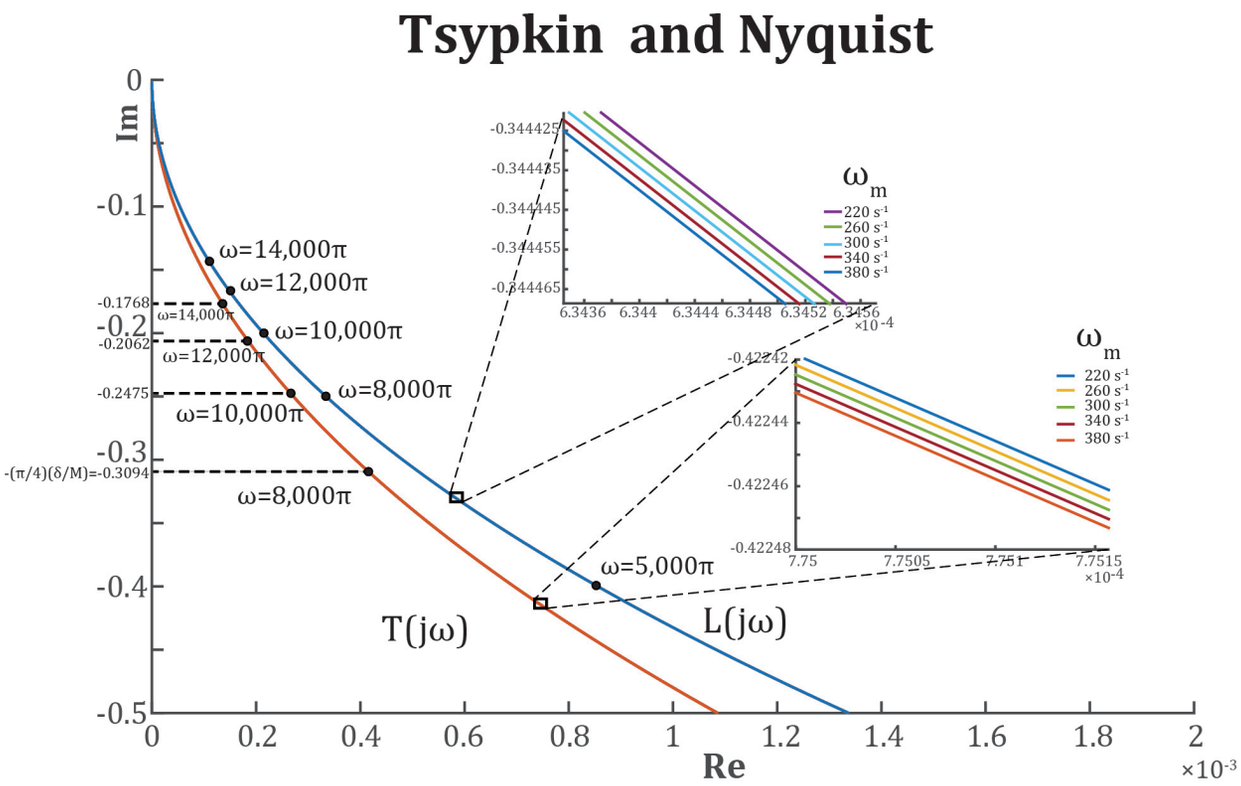


Figure 6. Graphical solution using Tsypkin's method.

Nominal power = 2 MW
Voltage = 690 V / 50 Hz
DC-link voltage = 1200 V
Stator/rotor turns ratio = 1/2
Mutual inductance (L_m) = 2.5 mH
Stator inductance (L_s) = 2.58 mH
Rotor inductance (L_r) = 2.58 mH
Stator resistance (R_s) = 2.6 mΩ
Rotor resistance (R_r) = 2.9 mΩ|
Pole pairs (P) = 2

Table 1. Machine parameters used in simulation.

$$\delta_{Q_s} = \frac{3L_m v_{sq}}{2L_s}\delta; \qquad \delta_{T_{em}} = \frac{3PL_m\lambda_{sd}}{2L_s}\delta \tag{40}$$

Moreover, as can be seen from **Figure 6** and Eqs. (38) and (39), the addition of hysteresis can be used to attenuated chattering since the hysteresis width is directly proportional to amplitude of chattering while it is inversely proportional to the frequency.

4.3. Step-by-step design

The design of the SMC proposed in this section can be summarized in the next step-by-step algorithm:

1. Select the sliding mode surfaces for torque and reactive power using Eq. (20).

2. Choose the gains, M_d and M_q, of the controller in Eq. (26) using the conditions given in Eq. (33) to guarantying robustness.

3. Compute a hysteresis value for the torque and reactive power controllers (sign functions) using Eqs. (40) to ensure an acceptable switching frequency in the power electronics.

Then, following the step-by-step process described in this subsection, a robust SMC to regulate torque and reactive power in DFIG systems can be designed. Furthermore, practical implementation is considered in the design since a method to compute a hysteresis value, limiting undesired high frequency commutation in power electronics, is provided.

5. Complex power and torque under unbalanced conditions

The active and reactive power can be obtained from electrical quantities seen from a stationary reference frame:

$$P_s = \frac{3}{2}\mathrm{Re}\left(\vec{v_s}\,\overrightarrow{\overline{i_s}}\right) = \frac{3}{2}\left(v_{s\alpha}i_{s\alpha} + v_{s\beta}i_{s\beta}\right) \tag{41}$$

$$Q_s = \frac{3}{2}\mathrm{Im}\left(\vec{v_s}\,\overrightarrow{\overline{i_s}}\right) = \frac{3}{2}\left(v_{s\beta}i_{s\alpha} - v_{s\alpha}i_{s\beta}\right) \tag{42}$$

where the operator $\overrightarrow{\overline{x}}$ is the complex conjugate.

In case of unbalanced conditions, the symmetrical components methods can be used for simplifying analysis, since zero sequence does not produce complex power, only positive and negative sequences are analyzed:

$$\vec{v_s} = \vec{v}_{s_1} + \vec{v}_{s_2} = v_{s\alpha 1} + v_{s\alpha 2} + j\left(v_{s\beta 1} + v_{s\beta 2}\right) \tag{43}$$

$$\vec{i_s} = \vec{i}_{s_1} + \vec{i}_{s_2} = i_{s\alpha 1} + i_{s\alpha 2} + j\left(i_{s\beta 1} + i_{s\beta 2}\right) \tag{44}$$

Substituting (43) and (44) in Eqs. (41) and (42) yields:

$$P_s = \overbrace{\frac{3}{2}\left(v_{s\alpha 1}i_{s\alpha 1} + v_{s\beta 1}i_{s\beta 1}\right)}^{P_{s11}} + \overbrace{\frac{3}{2}\left(v_{s\alpha 1}i_{s\alpha 2} + v_{s\beta 1}i_{s\beta 2}\right)}^{P_{s12}} + \overbrace{\frac{3}{2}\left(v_{s\alpha 2}i_{s\alpha 1} + v_{s\beta 2}i_{s\beta 1}\right)}^{P_{s21}} + \overbrace{\frac{3}{2}\left(v_{s\alpha 2}i_{s\alpha 2} + v_{s\beta 2}i_{s\beta 2}\right)}^{P_{s22}} \tag{45}$$

$$Q_s = \overbrace{\frac{3}{2}\left(v_{s\beta 1}i_{s\alpha 1} - v_{s\alpha 1}i_{s\beta 1}\right)}^{Q_{s11}} + \overbrace{\frac{3}{2}\left(v_{s\beta 1}i_{s\alpha 2} - v_{s\alpha 1}i_{s\beta 2}\right)}^{Q_{s12}} + \overbrace{\frac{3}{2}\left(v_{s\beta 2}i_{s\alpha 1} - v_{s\alpha 2}i_{s\beta 1}\right)}^{Q_{s21}} + \overbrace{\frac{3}{2}\left(v_{s\beta 2}i_{s\alpha 2} - v_{s\alpha 2}i_{s\beta 2}\right)}^{Q_{s22}} \tag{46}$$

On the other hand, electromagnetic torque can be obtained using the well-known equation:

$$T_{em} = \frac{3P}{2}\mathrm{Im}\left(\vec{\lambda}_s\,\overrightarrow{\overline{i_s}}\right) \tag{47}$$

Using the symmetrical components theory, an unbalance condition can be modeled with invariant positive and negative sequence components; therefore, at steady state, the derivate term of Eqs. (4) and Eq. (5) are zero leading to the following positive and negative stator flux components:

$$\vec{\lambda}_{s1} = \frac{\vec{v}_{s1} - R_s\vec{i}_{s1}}{j\omega_s}; \qquad \vec{\lambda}_{s2} = \frac{\vec{v}_{s2} - R_s\vec{i}_{s2}}{-j\omega_s} \tag{48}$$

Substituting Eqs. (43) and (44) and (48) in (47):

$$T_{em} = \frac{3P}{2\omega_s}\mathrm{Re}\left[\vec{v}_{s1}\overrightarrow{\overline{i}_{s1}} + \vec{v}_{s1}\overrightarrow{\overline{i}_{s2}} - \vec{v}_{s2}\overrightarrow{\overline{i}_{s1}} - \vec{v}_{s2}\vec{i}_{s2} - R_s\left(\left|\vec{i}_{s1}\right|^2 - \left|\vec{i}_{s2}\right|^2\right)\right] \tag{49}$$

Comparing Eq. (50) with Eq. (45), it is easy to see that the same terms appear in both equations:

$$T_{em} = \frac{P}{\omega_s}\left[P_{s11} + P_{s12} - P_{s21} - P_{s22} + \frac{3R_s}{2}\left(\left|\vec{\imath}_{s2}\right|^2 - \left|\vec{\imath}_{s1}\right|^2\right)\right] \tag{50}$$

The terms P_{s12} and P_{s21} are the cause of oscillation in torque and power when an unbalanced dip occurs. Since the condition for canceling torque oscillations ($P_{s12} = P_{s21}$) is opposite to the condition for canceling active power oscillations ($P_{s12} = -P_{s21}$), it is not possible to cancel both at the same time. It is preferable to cancel torque oscillations; otherwise the mechanical components may be severely damaged. On the other hand, to cancel reactive power oscillations, the following condition must be met $Q_{s12} = -Q_{s21}$.

6. Simulation results

To test the controller, a DFIG was simulated using the parameters displayed in **Table 1**. The blades model surface is shown in **Figure 1** with gearbox ratio ($\eta = 85.8$) rotor radius ($r = 40$ m) and air density ($\rho = 1.25$ kg\m^3). The nominal wind speed of 12 m/s, the nominal tip speed ratio $\Lambda_{opt} = 7.9533$ and the maximum power coefficient is $C_{p,\max} = 0.4109$. The pitch controller is ideal chopping the extracted aerodynamic power to the nominal power (2 MW) for wind speed above the nominal value. Considering that the maximum switching frequency of the converter is 7000 Hz; from **Figure 6** the desired hysteresis width is $\delta = 90.04A$; therefore, $\delta_{Q_s} = 128 \times 10^3$ and $\delta_{T_{em}} = 811$.

The following electromagnetic torque reference is used for maintaining the tip-speed ratio at the optimal value without measuring wind speed:

$$T_{ref} = -\frac{\frac{1}{2}\pi\rho R^5 C_{p,\max}}{\Lambda_{opt}^2 \eta^3}\omega_m^2 \tag{51}$$

On the other hand, the reactive power reference is maintained at zero.

The wind speed profile is shown in **Figure 7** II, the wind speed was taken from real measurements reported by the Department of Wind Energy, Technical University of Denmark [19] with values oscillating in all the operational range of the wind speed.

The power extracted by the blades is shown in **Figure 7** III, during the high wind speed periods, the ideal pitch controller maintains the extracted power at the nominal value of 2 MW, while the mechanical speed is controlled during the rest of the time to optimize power extraction as shown in **Figure 7** IV. The rotor converter nominal power limits the operational speed of the wind turbine $P_r \approx sP_s$.

The references are followed even under unbalanced grid conditions, a two-phase voltage dip is simulated at the terminals of the electric machine, the voltage dip is 20% of the nominal value. In **Figure 7** I, it is displayed the detail of the voltage dip. The voltage dip starts at 95 seconds and ends at 98 seconds of the simulation, the time axis in **Figure 7** I is chopped from 95.05 to

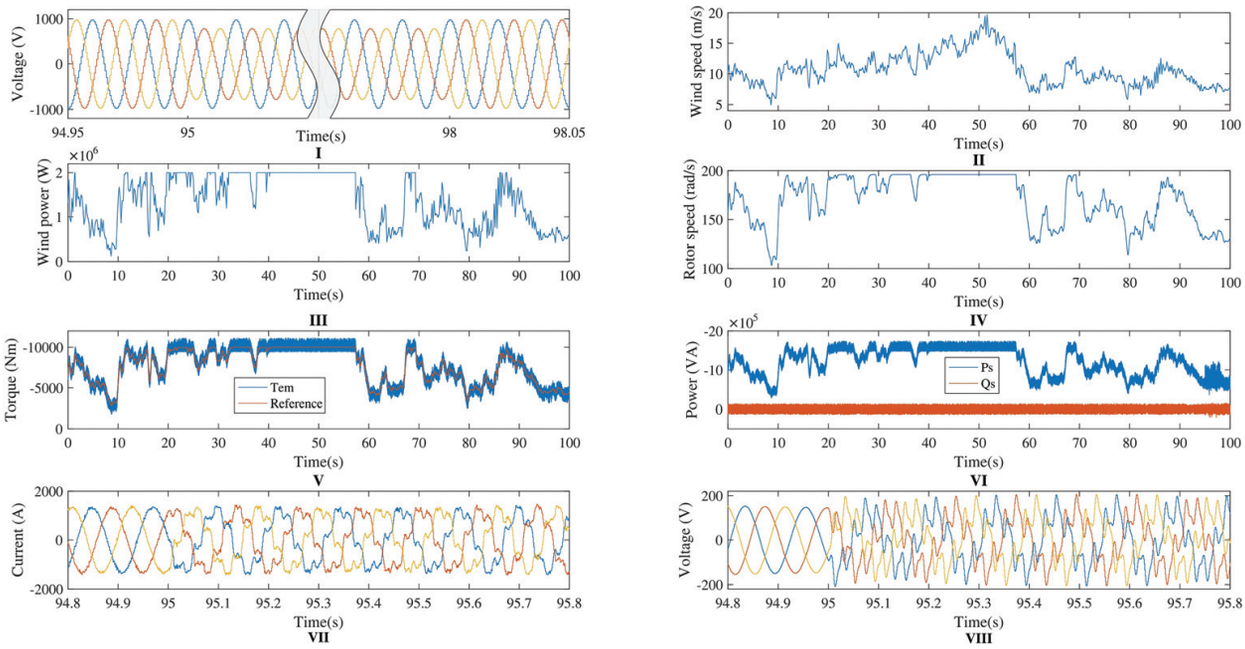


Figure 7. Simulation results: I stator voltage, II wind speed profile, III extracted aerodynamic wind power, IV rotor speed, V electromagnetic torque, VI stator active and reactive power, VII rotor current, VIII rotor filtered voltage.

97.95 s, in order to better see the stator voltage waveform during the fault. As demonstrated in Section 5, it is not possible to maintain both torque and reactive power constant during unbalanced conditions; therefore, the stator reactive power is affected (see **Figure 7** VI) since the controller forces the electromagnetic torque to be constant. As a result, the controller injects a negative sequence current to the rotor in order to cancel torque oscillations out (see **Figure 7** VII), it is worth mention that other control strategies as vector control requires a double control loop for controlling positive and negative sequence separated [13], which not only complicates the current regulation algorithm but also requires sequence decoupling of rotor current, a very complex issue that is avoided by using a robust control strategy.

Finally, the filtered rotor voltage is displayed in **Figure 7** VIII. The controller does not require modulation and automatically injects negative sequence voltage to regulate torque and reactive power under unbalanced conditions.

7. Conclusions

A stator-flux–oriented sliding mode control, which regulates torque and reactive power in DFIG, is presented. The controller is not dependent on electric machine parameters and do not require modulation, injecting the desired voltage vector directly to a two-level power converter. Despite the proposed SMC controller has a variable switching frequency, which is not desired in practical applications, the switching frequency is limited by a hysteresis loop in the torque and reactive power controllers. The hysteresis value is calculated by means of the frequency domain characterization of the DFIG system with SMC, via Tsypkin's method.

http://dx.doi.org/10.5772/intechopen.70714

Then, the safe operation of the power converter regarding commutation frequency is ensured. Furthermore, the proposed SMC is capable to reject stator flux variations providing a desired operation even under unbalanced grid conditions. Compared with classical control techniques as DTC, the presented SMC does not require the modification of the control loop. The equations for compute the control gains that ensure robustness and existence of SMC are given. Simulations validating the advantages of the proposed SMC are shown.

Nomenclature

v	Voltage [V]
i	Current [A]
λ	Magnetic flux [Wb]
s, r	Stator, rotor sub index
d, q	Direct, quadrature reference frame axis component
α, β	Alpha, beta reference frame axis component
L_m	Magnetic inductance [H]
L_s	Stator inductance [H]
L_r	Rotor inductance [H]
P	Number of pole pairs.
P_s, Q_s	Stator active, reactive power [W, VA]
T_{em}	Electromagnetic torque [N·m]
V_{DC}	DC-link voltage [V]
ω_s	Synchronous speed [rad/s]
θ_{sf}	Stator flux angular position [rad]
ω_m	Rotor speed [rad/s]
θ_m	Rotor mechanical angle [rad]
ω_r	Rotor electrical speed [rad/s]
s	Slip
P_{wind}	Aerodynamic power [W]
C_P	Power coefficient
γ	Pitch angle [deg]
Λ	Tip-speed ratio

ρ Air density [kg/m^3]

A Turbine transverse area [m^2]

r Turbine radius [m]

V Wind speed [m/s]

η Gearbox ratio

s Complex frequency variable

Author details

Ivan Villanueva*, Antonio Rosales, Pedro Ponce and Arturo Molina

*Address all correspondence to: ivan.villanueva@itesm.mx

Tecnologico de Monterrey, Mexico

References

[1] GWEC. Global Wind Report 2016 [Internet]. 2017. Available from: http://www.gwec.net/publications/global-wind-report-2/global-wind-report-2016/# [Accessed: 07/17/2017]

[2] European Commission. JRC Wind Energy Status Report: 2016 Edition [Internet]. March 2017. Available from: https://ec.europa.eu/jrc/en/news/jrc-wind-energy-status-report-2016-edition [Accessed: 07/17/2017]

[3] Tapia A, Tapia G, Ostaloza JX, Saenz JR. Modeling and control of a wind turbine driven doubly fed induction generator. IEEE Transactions on Energy Conversion. 2003;**18**(2):194-204

[4] Xu L, Wang Y. Dynamic modeling and control of DFIG-based wind turbine under unbalanced network conditions. IEEE Transactions on Power Systems. 2007;**22**(1):314-323

[5] Abad G, Rodriguez MA, Poza J, Canales M. Direct torque control of doubly fed induction machine-based wind turbines under voltage dips and without crowbar protection. IEEE Transactions on Energy Conversion. 2012;**25**(2):586-588

[6] Ong CM. Dynamic Simulation of Electric Machinery Using Matlab/Simulink. Prentice Hall: Upper Saddle River, NJ; 1998. 626 p

[7] Lubosny Z. Wind Turbine Operation in Electric Power Systems. Springer; 2003. 262 p

[8] Abad G, Lopez J, Rodriguez M, Marroyo L, Iwanski G. Doubly Fed Induction Machine: Modeling and Control for Wind Energy Generation. John Wiley & Sons: Hoboken, NJ; 2011. 625 p

[9] Utkin V, Guldner J, Shi J. Sliding Mode Control in Electro-Mechanical Systems. 2nd ed. CRC Press; Boca Raton, Florida, 2009. p. 503

[10] Venkataramanan R. Sliding Mode Control of Power Converters [Dissertation]. California Institute of Technology; Pasadena, California, 1986

[11] Villanueva I, Rosales A, Ponce P, Molina A. Stator-flux-oriented sliding mode controller for DFIG with variable hysteresis loop for limiting switch frequency of rotor-side power converter. In: IEEE, editor. Industrial Technology (ICIT), 2017 IEEE International Conference; 2017

[12] Gelb A, Vander Velde WE. Multiple-Input Describing Functions and Nonlinear System Design. New York: McGraw-Hill; 1968. 655 p

[13] Xu L. Coordinated control of DFIG's rotor and grid side converters during network unbalance. IEEE Transactions on Power Electronics. 2008;**23**(3):1041-1049

[14] Gupta G, Gosh A. Frequency-domain characterization of sliding mode control of an inverter used in DSTATCOM application. IEEE Transactions on Circuits and Systems. 2006;**53**(3):662-672

[15] Martinez MI, Tapia G, Susperregui A, Camblong H. Sliding mode control for DFIG rotor and grid side converters under unbalanced and harmonically distorted grid voltage. IEEE Transactions on Energy Conversions. 2012;**27**(2):328-339

[16] Beltran B, Benbouzid M, Ahmed-Ali T. High-order sliding mode control of a DFIG-based wind turbine for power maximization and grid fault tolerance. In: Electric Machines and Drives Conference; IEEE; 2009. p. 183-189

[17] Benbouzid M, Beltran B, Amirat Y, Yao G, Han J, Mangel H. Second order sliding mode control of DFIG-based wind turbines fault ride through capability enhancement. ISA Transactions. 2014;**53**(3):827-833

[18] Martinez M, Susperregui A, Tapia G, Xu L. Sliding mode control of a wind turbine driven double-fed induction generator under non-ideal grid voltages. IET Renewable Power Generation. 2013;**7**(4):370-379

[19] Hansen KS, Larsen GC. Database of Wind Characteristics [Internet]. Available from: http://www.winddata.com/ [Accessed: January 2016]

IntechOpen

IntechOpen